Fingering instability of a sheet of yield-stress fluid

John R. de Bruyn, Piotr Habdas, and Stella Kim
Department of Physics and Physical Oceanography, Memorial University of Newfoundland, St. John's, Newfoundland, Canada A1B 3X7
(Received 4 January 2002; published 20 September 2002)

We study the fingering instability that occurs at the contact line of a thin sheet of a yield-stress fluid flowing down an incline. We derive an expression for the wavelength of the finger pattern as a function of inclination angle for a Herschel-Bulkley fluid. The wavelength is predicted to diverge at a finite angle which is related to the yield stress of the fluid. We also measure the wavelength of the finger pattern with suspensions of bentonite clay in water. Our experimental results agree well with the theoretical prediction.

DOI: 10.1103/PhysRevE.66.031504 PACS number(s): 83.60.La, 83.60.Wc, 83.80.Hj, 47.54.+r

I. INTRODUCTION

When a viscous fluid sheet spreads under the influence of an external force, the fluid-solid-air contact line at the front of the sheet can become unstable to the formation of fingers [1–20]. This instability has been studied in several contexts, including gravity-driven flow down an incline [1–14] centrifugal forcing (spin coating) [15–18], and forcing by Marangoni forces [19,20]. In practical terms, this type of instability is important in many situations, including coating applications [21], granular flows [22], and lava flows [23]. Most previous studies of contact line instabilities have considered only Newtonian fluids, although Homsy and coworkers have studied fingering in the spin coating of viscoelastic fluids [16–18], and Saffman-Taylor fingering has been studied in yield-stress fluids [24,25] and other non-Newtonian materials [26]. On the other hand, in many situations of practical interest [21–23], the fluids involved are non-Newtonian.

Figure 1 is a schematic illustration of a sheet of viscous fluid flowing down an inclined plane. In an ''outer'' region, far from the contact line, surface tension plays no role, and the film thickness in this region has been described by Huppert [1]. Near the contact line in an ''inner'' region, however, surface tension dominates [4–7]. The free surface of the film forms a capillary ridge near the contact line, and it has been shown that this ridge is unstable to perturbations in a range of wave numbers [4,11,12]. Surface tension is crucial for the initial instability [3], which leads to variations in the depth of the ridge. The subsequent growth of the fingers is due to the fact that thicker regions of the ridge flow more easily under the action of the external force [10,18]. A different interpretation of the origin of the fingers that does not involve an instability is presented by Veretennikov *et al.* [13].

The wavelength and growth rate of the instability for Newtonian fluids have been calculated by Troian *et al.* [4] They defined a length scale ℓ, given by

$$\ell = \frac{H}{(3\,\mathrm{Ca})^{1/3}}, \tag{1}$$

where H is a characteristic depth of the fluid film, normally taken as the depth of the film where the inner and outer regions join. $\mathrm{Ca} = \eta U/\sigma$ is the capillary number, η is the (constant) viscosity of the fluid, U a characteristic flow velocity, and σ the surface tension. Troian *et al.* [4] performed a linear stability analysis on the capillary ridge and found the fastest growing unstable mode to have a wavelength of approximately 14ℓ. Experimental studies of the fingering instability in spin coating [16] and with Marangoni-forced contact lines [20] showed good agreement with theoretical predictions of the dominant wavelength of the finger pattern and the growth rate of the fingers. In the case of flow down an incline, the wavelength $\lambda \propto \sin\alpha^{-1/3}$ [1], where α is the angle of inclination. This angle dependence has been confirmed in experiments [1,2,8,9], but the measured wavelengths were roughly 50% smaller than predicted by the theory [9]. This discrepancy has been resolved to some extent by Brenner [10,12], who showed that the component of the gravitational force perpendicular to the plane, which was neglected in Ref. [4], was significant, and found that at small angles of inclination the wavelength was not constant in units of ℓ.

In all cases, the fluids studied previously flowed for arbitrarily small inclination angles. This will not be the case for fluids with a yield stress. As reviewed below, the maximum shear stress developed in the fluid layer due to the downslope component of gravity is proportional to the layer thickness and $\sin\alpha$. For α smaller than some critical inclination angle α_c, this will be less than the yield stress, and so the material will not flow. This fact has been exploited in ''inclined plane rheometers,'' [27–30] that are used to determine

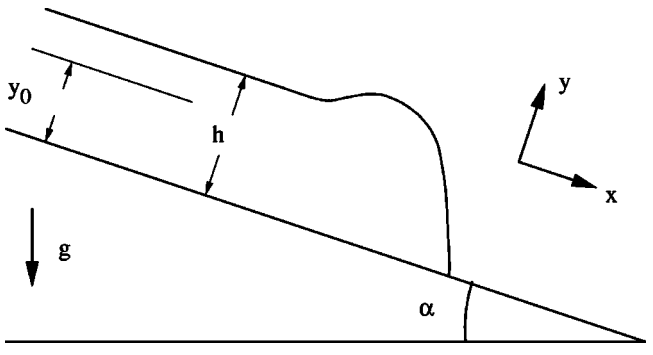

FIG. 1. A schematic diagram of a sheet of fluid flowing down a plane inclined at an angle α to the horizontal. The fluid thickness is h away from the contact line; y_0 is the level at which the stress in the fluid is equal to the yield stress.

the yield stress of a fluid either from the angle at which a layer of known thickness starts to flow, or from the layer depth at which the material stops flowing at a given inclination angle.

In this paper we study the fingering instability at the contact line of a sheet of yield-stress fluid flowing down an incline. As a result of the existence of a yield stress, the fluid does not flow for $\alpha \leqslant \alpha_c$, and when it does flow, the viscosity is a function of strain rate, and so for both inclination angle and position within the fluid. We first derive an expression for the length scale ℓ, and so of the wavelength of the finger pattern, as a function of inclination angle. We then present the results of experiments on suspensions of bentonite clay in water, and compare them with our theoretical predictions.

II. THEORY

We consider a sheet of yield-stress fluid on an incline as shown in Fig. 1. The angle of inclination is α, the fluid flows in the x direction, with the y direction being perpendicular to the plane. The finger pattern develops along the z direction, which is out of the plane of the paper. We assume laminar flow, and for simplicity we assume that the film has a uniform thickness h in the outer region. In this case the flow velocity u is in the x direction, and by symmetry, it depends only on y away from the contact line. These assumptions essentially ignore the subtleties of the free surface shape and the matching of the inner and outer regions [4,12], but are adequate for our purposes.

We do not perform a detailed analysis of the equations of motion for this system. Rather, we simply assume that the instability occurs, and that λ is proportional to the length scale ℓ. We derive an expression for ℓ and for the α dependence of the pattern wavelength, modifying the arguments of Ref. [4] to take into account the non-Newtonian properties of our fluid. These properties enter in the calculation of the capillary number Ca through the velocity U and the viscosity η. For a Newtonian fluid, η is constant by definition, but for a yield-stress fluid, η is a function of strain rate, and is infinite when the stress is below the yield stress.

We will use the Herschel-Bulkley model of a yield-stress fluid. For one-dimensional flow, such as we consider here, the Herschel-Bulkley constitutive relation is

$$\tau = \tau_c + K\dot{\gamma}^n, \quad \tau > \tau_c, \tag{2a}$$

$$\dot{\gamma} = 0, \quad \tau \leqslant \tau_c, \tag{2b}$$

where τ is the stress, τ_c the yield stress, $\dot{\gamma} = \partial u/\partial y$ the strain rate, and K and n are parameters that are typically determined by fitting Eq. (2a) to rheological data. The Bingham model is a special case of Eqs. (2) with $n=1$. Clay-water suspensions, like that used in the experiments described in Sec. III are reasonably well characterized by Eqs. (2) with $n \approx 1/3$ [30].

The problem of uniform laminar flow of a layer of yield-stress fluid on an incline has been studied previously [28–33]. In the outer region, away from the contact line, the steady state stress in the layer is due to the component of the gravitational force in the x direction, and is a function of y only. It is given by

$$\tau(y) = \rho g (h-y) \sin\alpha, \tag{3}$$

where ρ is the fluid density, g is the acceleration due to gravity, and we have used the no-stress boundary condition $\tau = 0$ at the free surface $y = h$. The stress is maximum at $y = 0$, where it is equal to

$$\tau(0) = \rho g h \sin\alpha. \tag{4}$$

For flow to occur, this must be greater than the yield stress. This allows us to define a critical angle α_c, below which flow does not occur for a layer of thickness h:

$$\sin\alpha_c = \tau_c / \rho g h. \tag{5}$$

If $\tau(0) > \tau_c$, then the fluid will be sheared from $y=0$ up to a level $y = y_0$ at which the stress is equal to τ_c. For $y_0 < y \leqslant h$ the stress is less than τ_c and the fluid is not sheared. The unsheared region has a thickness h_0, where

$$h_0 = \tau_c / \rho g \sin\alpha. \tag{6}$$

The thickness of the layer h is equal to $y_0 + h_0$, so

$$y_0 = h - h_0 = h - \frac{\tau_c}{\rho g \sin\alpha} \tag{7a}$$

$$= \frac{h}{\sin\alpha}(\sin\alpha - \sin\alpha_c). \tag{7b}$$

To determine ℓ for our fluid layer, we need expressions for the characteristic velocity U and the viscosity η. We get the velocity $u(y)$ in the layer by rewriting Eq. (2) as

$$\dot{\gamma} = du/dy = \left(\frac{\tau - \tau_c}{K}\right)^{1/n} \tag{8}$$

for $\tau > \tau_c$. Integrating this with the no-slip boundary condition $u(0) = 0$, we get [30]

$$u(y) = \left(\frac{\rho g \sin\alpha}{K}\right)^{1/n} \frac{1}{1+(1/n)} \left[y_0^{1+(1/n)} - (y_0 - y)^{1+(1/n)}\right] \quad \text{for } y < y_0 \tag{9}$$

and

$$u(y) = u(y_0) = \left(\frac{\rho g \sin\alpha}{K}\right)^{1/n} \frac{1}{1+(1/n)} y_0^{1+(1/n)} \quad \text{for } y \geqslant y_0. \tag{10}$$

The viscosity η of the fluid is

$$\eta = \tau/\dot{\gamma} = \frac{\tau_c}{\dot{\gamma}} + K\dot{\gamma}^{n-1}. \tag{11}$$

This depends on $\dot{\gamma}$ and y. For our purposes we need only a characteristic viscosity, so we take $\dot{\gamma} \approx u(y_0)/y_0$ in Eq. (11), which gives

$$\eta = \frac{\tau_c y_0}{u(y_0)} + K\left(\frac{u(y_0)}{y_0}\right)^{n-1}. \tag{12}$$

Taking the characteristic velocity U to be $u(y_0)$ and using Eqs. (7b) and (10), we have

$$\eta U = \eta u(y_0) = \tau_c y_0 + \frac{K u(y_0)^n}{y_0^{n-1}} \tag{13}$$

$$= \frac{\rho g h^2}{\sin\alpha}\left[\sin\alpha_c(\sin\alpha - \sin\alpha_c) + \left(\frac{1}{1+(1/n)}\right)^n \times (\sin\alpha - \sin\alpha_c)^2\right]. \tag{14}$$

Using the constant layer thickness h as the characteristic thickness and substituting Eq. (14), into Eq. (1), we end up with an expression for ℓ for our Herschel-Bulkley fluid:

$$\ell = \left(\frac{\sigma h \sin\alpha}{3\rho g}\right)^{1/3} \frac{1}{\left[\sin\alpha_c(\sin\alpha - \sin\alpha_c) + \left(\frac{1}{1+(1/n)}\right)^n (\sin\alpha - \sin\alpha_c)^2\right]^{1/3}}. \tag{15}$$

For a Newtonian fluid, $\alpha_c = 0$ and $n = 1$, and Eq. (15) reduces to

$$\ell = \left(\frac{\sigma h}{3\rho g \sin\alpha}\right)^{1/3}, \tag{16}$$

which recovers the α dependence found previously for that case [1,4].

Assuming that λ is proportional to ℓ [4], which should be the case as long as α is not close to zero [10], Eq. (15) shows that λ diverges at the critical angle α_c and approaches a finite value at $\alpha = 90°$. Note that ℓ does not depend strongly on the rheology of the fluid, except through the critical inclination angle α_c, which is proportional to the yield stress. ℓ is independent of K, and depends on n only through the coefficient $1/[1+(1/n)^n]$ in the second term of the denominator. This coefficient is always of order 1, varying from 1 for $n = 0$ to 0.3688 for $n \to \infty$.

III. EXPERIMENT

Fingering experiments were done by flowing a fixed quantity of fluid down an incline. We used suspensions of bentonite clay in water. The bentonite was used as obtained from the supplier (Fisher Scientific). The size distribution of the bentonite powder was determined using the sedimentation method, in which the particle sizes were determined from their stationary falling velocity in water. The maximum particle diameter was approximately 4 μm.

The bentonite was mixed with deionized water at concentrations of 6%, 7%, and 8% bentonite by weight. The suspensions were mixed for 15 min with an Arrow 1750 mixer, then for 10 min with a hand-held kitchen blender, and then with the Arrow mixer for another 5 min. The suspension was mixed again with the Arrow mixer for 5 min immediately before starting a run.

Our experimental apparatus consisted of a 61 cm by 104 cm sheet of float glass mounted on an aluminum frame that allowed the glass sheet to be tilted to both positive and negative inclination angles. Prior to each run, the glass surface was cleaned with deionized water and then wiped clean with paper towels. The surface was tilted to a fixed negative angle and 250 ml of the experimental fluid was poured evenly into the downhill end. The fluid was allowed to sit for 5 minutes, after which the glass surface was tilted quickly and smoothly to the desired positive angle α. At small α, the fluid sheet did not flow at all, since the maximum stress in the fluid sheet did not exceed the yield stress. For $\alpha > \alpha_c$ flow did occur. Fingering was observed at the front of the fluid sheet for all runs in which flow occurred. A video camera mounted above the plane and interfaced to a personal computer recorded images of the flowing sheet at a preselected time interval.

An example of the fingering patterns observed is shown in Fig. 2. Typically, the fingers nearest to the edges of the plane form sooner and grow to be longer than the others due to the boundary conditions at the edges, but this seemed to have

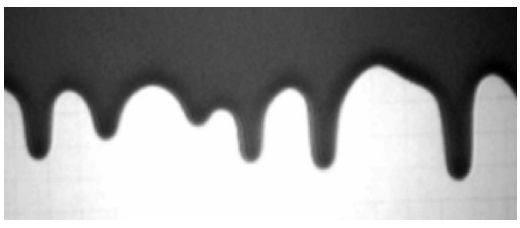

FIG. 2. Fingers at the contact line of a sheet of a suspension of 6% bentonite by weight in water. Here $\alpha = 21.5°$ and the raised end of the plane is at the top of the figure. The field of view is 39.8 cm in the horizontal direction.

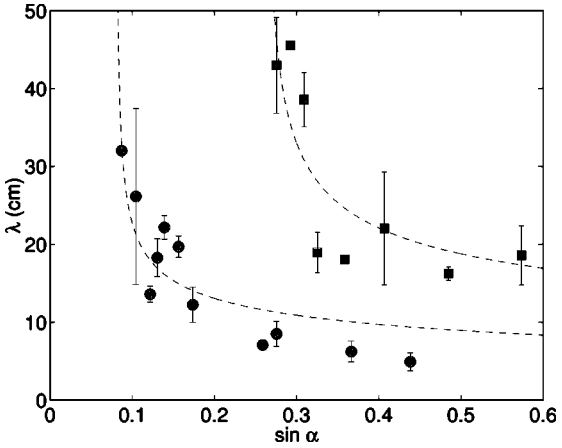

FIG. 3. The measured wavelength of the finger pattern plotted as a function of $\sin\alpha$ for 6% (circles) and 8% (squares) bentonite-water suspensions. The dashed lines are fits to the theoretical expression, Eq. (17).

little effect on the spacing between adjacent fingers. The pattern wavelength λ was measured directly from the recorded video images at the earliest time at which the fingers were clearly identifiable. The wavelength was not perfectly uniform, with the standard deviation in λ being typically approximately 20%. This variation in λ is similar to what has been found in experiments on Newtonian fluids [9].

The measured wavelengths are plotted as a function of $\sin\alpha$ in Fig. 3 for the 6% and 8% bentonite suspensions. The results for the 7% suspension lay in between the two data sets shown. The wavelengths plotted have been averaged over all fingers in an image and often averaged over two or more runs at the same angle. The error bars are standard deviations. Also plotted are fits of the data to the form predicted by the theory given above,

$$\lambda = \frac{A_1 \sin\alpha^{1/3}}{\{\sin\alpha_c(\sin\alpha - \sin\alpha_c) + A_2(\sin\alpha - \sin\alpha_c)^2\}^{1/3}}, \tag{17}$$

with $\sin\alpha_c$ and A_1 free parameters. The coefficient A_2 was fixed at 0.63 (the expected value of the factor $1/[1+(1/n)]^n$ for $n=\frac{1}{3}$). The agreement between the data and the fits is quite good, although the theory perhaps overestimates the wavelength at higher angles for the 6% data. Varying the value of A_2 between 0.63 and 1 did not dramatically change the quality of the fit, and caused the other parameters to change by less than their uncertainty. On the other hand, setting $A_2=0$, that is, removing the second term in the denominator of Eq. (17), made the fits significantly worse, and making A_2 large did not improve the agreement at high α.

The values of the fit parameters obtained for the three concentrations studied are given in Table I. Of most interest is $\sin\alpha_c$, from which the yield stress can be determined. We estimate the initial thickness of the fluid layer from the volume and the length of the fluid sheet as poured, and using Eq. (5) we obtain the values of the yield stress listed in the fourth column of Table I. These values of τ_c are in good agreement with the rheological data of Ref. [24], but somewhat higher than those measured by us with a cone and plate rheometer.

TABLE I. Parameters and yield stress obtained from fits of the experimental data to Eq. (17).

Concentration (%)	A_1 (cm)	$\sin\alpha_c$	τ_c (Pa)[a]
6	5.9 ± 0.6	0.081 ± 0.003	2.22
7	5.6 ± 0.7	0.151 ± 0.003	5.69
8	10.9 ± 1.5	0.262 ± 0.009	17.0

[a]From Eq. (5).

IV. DISCUSSION

The theoretical expression for the length scale ℓ given by Eq. (15) describes our wavelength data well. In particular, the prediction that the wavelength diverges at the critical angle α_c is borne out by the data, and the values of α_c determined from the fits give yield stresses consistent with published values [24]. Because ℓ is proportional to $U^{-1/3}$, it is not surprising that the wavelength of the finger pattern diverges when the flow stops for both yield-stress and Newtonian fluids. However, the situation is different in the two cases: for Newtonian fluids, the flow stops because there is no driving force for $\alpha=0$, while in the case considered here flow stops at $\alpha=\alpha_c$ because the fluid's viscosity becomes infinite there.

From Eq. (15), we expect the fitting parameter A_1 to be proportional to $(\sigma h/3\rho g)^{1/3}$. Estimating this quantity and comparing it to the values of A_1 shown in Table I suggests that $\lambda\approx 35\ell$, with the constant of proportionality being somewhat larger for the 8% data. Neither ρ nor σ vary much over the range of concentrations studied here, but the 8% layer was thicker by roughly a factor of 2 than the two less concentrated layers due to the higher viscosity and yield stress of the 8% fluid. This accounts at least partly for the increase. For a Newtonian fluid, de Bruyn found $\lambda\approx 9.4\ell$ [9] from similar experiments over a range of inclination angles.

We emphasize that our theoretical prediction does not come from a complete stability analysis of the equations of motion for a sheet of Herschel-Bulkley fluid flowing down an incline, but is rather an approximation based on an extension of the results derived for Newtonian fluids [4]. We have ignored any variation in depth of the sheet and the rather subtle physics that pertains near the contact line [4,12]. We have not tried to estimate the growth rate of the fingering instability; this would have to come from an analysis of the equations of motion.

ACKNOWLEDGMENTS

This research was supported by the Natural Sciences and Engineering Research Council of Canada. We are grateful to J. Wylie for useful discussions, A. Marangoni and G. Mazzanti for rheological assistance, and H. Gillespie for measuring the particle size distribution.

[1] H.E. Huppert, Nature (London) **300**, 427 (1982).
[2] N. Silvi and E.B. Dussan V, Phys. Fluids **28**, 5 (1985).
[3] L.W. Schwartz, Phys. Fluids A **1**, 443 (1989).
[4] S.M. Troian, E. Herbolzheimer, S.A. Safran, and J.F. Joanny, Europhys. Lett. **10**, 25 (1989).
[5] L.M. Hocking, J. Fluid Mech. **221**, 373 (1990).
[6] R. Goodwin and G.M. Homsy, Phys. Fluids A **3**, 515 (1991).
[7] J.A. Moriarty, L.W. Schwartz, and E.O. Tuck, Phys. Fluids A **3**, 733 (1991).
[8] J.M. Jerrett and J.R. de Bruyn, Phys. Fluids A **4**, 234 (1992).
[9] J.R. de Bruyn, Phys. Rev. A **46**, R4500 (1992).
[10] M.P. Brenner, Phys. Rev. E **47**, 4597 (1993).
[11] L.M. Hocking and M.J. Miksis, J. Fluid Mech. **247**, 157 (1993).
[12] A.L. Bertozzi and M.P. Brenner, Phys. Fluids **9**, 539 (1997).
[13] I. Veretennikov, A. Indeikina, and H.-C. Chang, J. Fluid Mech. **373**, 81 (1998).
[14] M.F.G. Johnson, R.A. Schluter, M.J. Miksis, and S.G. Bankoff, J. Fluid Mech. **394**, 339 (1999).
[15] F. Melo, J.F. Joanny, and S. Fauve, Phys. Rev. Lett. **63**, 1958 (1989).
[16] N. Fraysse and G.M. Homsy, Phys. Fluids **6**, 1491 (1994).
[17] M.A. Spaid and G.M. Homsy, J. Non-Newtonian Fluid Mech. **55**, 249 (1994).
[18] M.A. Spaid and G.M. Homsy, Phys. Fluids **8**, 460 (1996).
[19] A.M. Cazabat, F. Heslot, S.M. Troian, and P. Carles, Nature (London) **346**, 824 (1990).
[20] J.B. Brzoska, F. Brochard-Wyart, and F. Rondelez, Europhys. Lett. **19**, 97 (1992).
[21] K.J. Ruschak, Annu. Rev. Fluid Mech. **17**, 65 (1985).
[22] O. Pouliquen, J. Delour, and S.B. Savage, Nature (London) **386**, 816 (1997).
[23] R.W. Griffiths and J.H. Fink, J. Fluid Mech. **347**, 13 (1997).
[24] H. van Damme, C. Laroche, and L. Gatineau, Rev. Phys. Appl. **22**, 241 (1987). Note that the concentrations in Table I of this reference are given as the ratio of clay weight to water weight, while ours are given as the ratio of clay weight to total mixture weight.
[25] P. Coussot, J. Fluid Mech. **380**, 363 (1999).
[26] K.V. McCloud and J.V. Maher, Phys. Rep. **260**, 139 (1995).
[27] G. Astarita, G. Marrucci, and G. Palumbo, Ind. Eng. Chem. Fundam. **3**, 333 (1964).
[28] D. De Kee, R.P. Chhabra, M.B. Powley, and S. Roy, Chem. Eng. Commun. **96**, 229 (1990).
[29] P. Coussot and S. Boyer, Rheol. Acta **34**, 534 (1995).
[30] P. Coussot, *Mudflow Rheology and Dynamics* (Balkema, Rotterdam, 1997).
[31] P.R. Paslay and A. Slibar, Trans. Soc. Rheol. **2**, 255 (1958).
[32] C.D.D. Howard, J. Hydraul. Div., Am. Soc. Civ. Eng. **HY5**, 89 (1963).
[33] P. Coussot, J. Hydraul. Res. **32**, 535 (1994).